Cold-target electron-ion-coincidence momentum-spectroscopy study of electron-impact single and double ionization of N_2 and O_2 molecules

Shaokui Jia,[1] Jiaqi Zhou,[1] Xing Wang,[1,*] Xiaorui Xue,[1] Xintai Hao,[1] Qingrui Zeng,[1] Yongtao Zhao,[1] Zhongfeng Xu,[1] Alexander Dorn,[2] and Xueguang Ren[1,†]

[1]*Ministry of Education Key Laboratory for Nonequilibrium Synthesis and Modulation of Condensed Matter, School of Physics, Xi'an Jiaotong University, Xi'an 710049, China*

[2]*Max-Planck-Institut für Kernphysik, Saupfercheckweg 1, 69117 Heidelberg, Germany*

(Received 6 December 2022; accepted 6 March 2023; published 20 March 2023)

We report experimental studies of electron-impact ionization of nitrogen (N_2) and oxygen (O_2) molecules using a cold target recoil ion momentum spectrometer (COLTRIMS, reaction microscope). The recoil ion is detected in coincidence with one outgoing electron such that the momentum vectors and consequently the kinetic energies for these final-state particles are determined. The ionization cross sections for producing the doubly and singly charged parent ions were measured as a function of the incident electron energy ranging from 50 to 600 eV. For molecular dications, e.g., O_2^{2+}, the cross sections are obtained by measuring both the ion time of flight and two-dimensional position spectra, which is demonstrated to be an efficient way to suppress the contribution of the dissociation channels with the O^+ products as both ions have the identical mass-to-charge ratios. The projectile energy-loss spectra correlated to the final-state ions are obtained, which provide direct evidence of the ionization mechanisms of N_2 and O_2 molecules. It is found that the O_2^{2+} dication is produced mainly by Auger process after single ionization in $2\sigma_g$ inner-valence shell of O_2 molecule, while the N_2^{2+} dication is generated by the direct removal of two electrons from the outermost $3\sigma_g$ orbital of N_2 molecule.

DOI: 10.1103/PhysRevA.107.032819

I. INTRODUCTION

Electron-impact ionization of atoms and molecules plays an important role in a range of research fields, such as quantum few-body dynamics [1,2], radiation biology and chemistry [3–6], plasma physics [7,8], and interstellar chemistry [9–12]. In particular, molecular double ionization in the gas phase has attracted extensive interest due to the universality of cationic radicals in interstellar medium (ISM) [13,14]. As indicators of energetic processes, dications could play a significant role in atmospheric escape and induce new types of chemical reactions [10]. Although numerous studies have been devoted to reveal the formation processes of doubly charged molecular ions, the understanding of the detailed mechanisms and dynamics remains very incomplete due to the intrinsic complexity of the ionization reactions.

The dications can be formed by direct double ionization (DI), in which two outer-valence electrons are ejected simultaneously, or a indirect process via inner-valence ionization and subsequent autoionization, i.e., Auger process [15–18]. One promising way of characterizing the DI mechanisms and dynamics of atoms and molecules is to measure total and differential cross sections of the dications, which are often compared with the results of other products, e.g., singly charged ions [19–34]. The cross-section measurements generally rely on the detection of ion time of flight (TOF) to discriminate between specific products according to their mass-to-charge (m/q) ratios. For ionization of molecules, there can be dissociation channels, which make it difficult to distinguish between the intact dications and singly charged fragment ions due to their identical m/q ratios, e.g., O_2^{2+} and O^+ or $C_6H_6^{2+}$ and $C_3H_3^+$ ions [30–32]. Therefore, we need to exclude the possible contributions of fragmented ions in order to determine accurately the cross sections for the doubly charged parent ions.

In previous studies, several techniques have been developed to measure the ionization cross sections for producing the doubly and singly charged parent ions, such as the experiments with heteroisotopic molecules, cycloidal mass spectrometer, delayed extraction TOF technique, and velocity map imaging method [25–30]. As the most abundant components of the Earth's atmosphere, nitrogen (N_2) and oxygen (O_2) molecules are regarded as two benchmark targets whose ionization cross sections have been studied extensively for understanding the reaction mechanisms and dynamics [26–28,30,33,34]. Among them, the cross sections for N_2^{2+} show good agreement between different experiments. However, there exist considerable discrepancies in both magnitude and tendency for the O_2^{2+} cross sections [26–28,30]. One possible reason is that the fragment O^+ ions are not completely separated from the O_2^{2+} yields, which remains a challenging problem, and calls for more clarifications and experimental studies with additional methods.

In the present work, electron-impact ionization of N_2 and O_2 molecules is investigated with cold target recoil ion momentum spectroscopy (COLTRIMS) [35,36]. Final-state products involving the scattered projectile electron and recoil ion are detected with an electron-ion double-coincidence

*wangxingcn@xjtu.edu.cn
†renxueguang@xjtu.edu.cn

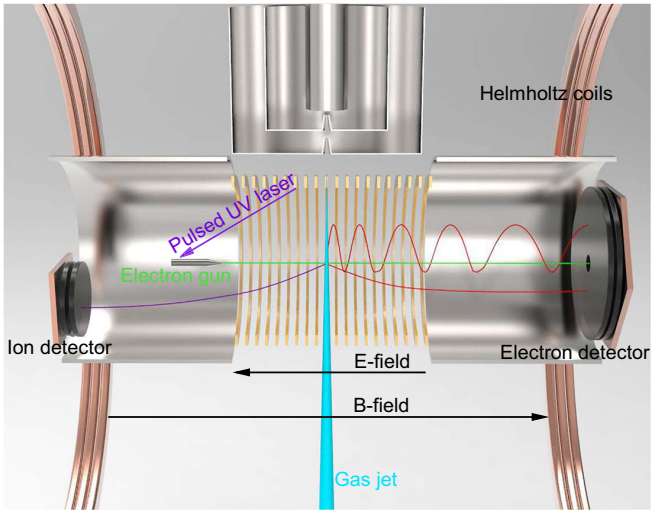

FIG. 1. Schematic diagram of the experimental apparatus: COLTRIMS reaction microscope with electron projectile beam.

method. To solve the problem mentioned above, we develop an approach to efficiently suppress the contributions of singly charged fragment ions from the intact dications, which can be regarded as a general way to determine the cross sections of doubly charged parent ions, in particular for the ionization of molecules like O_2, N_2, C_2H_4, C_6H_6, and so on. We efficiently separate singly charged molecular dissociation products from doubly charged parent ions by their high momenta from the dissociation processes. The cross-section ratios between doubly and singly charged parent ions for N_2 and O_2 molecules are measured in the energy range of 50–600 eV with high resolution and excellent signal-to-noise ratio. In addition, we determine the projectile energy-loss spectra correlated to ion production, which can provide more insight into the ionization mechanisms of the electron-impact processes [37–39].

II. EXPERIMENTAL DETAILS

The experiments were performed using a COLTRIMS reaction microscope combined with a photoemission electron source [35,36,40]. The schematic diagram of the setup is shown in Fig. 1, where a well-focused ($\approx$1-mm-diameter) pulsed electron beam crosses perpendicularly with a supersonic cold gas jet formed by a 30-μm nozzle and a two-stage differential pumping system. The pulsed electron beam is produced by a photoemission electron gun with a tantalum photocathode, which is irradiated by ultraviolet-light pulses with frequency of 40 kHz, wavelength of 266 nm, and pulse width of 0.5 ns. The vacuum of the reaction chamber was maintained at around 10^{-10}–10^{-9} mbar, and thus we can obtain an excellent signal-to-noise ratio for the final-state products.

The final-state ions and electrons created in the reaction region for each ionization event are accelerated and guided by homogeneous electric (2 V/cm) and magnetic fields (8 Gauss) to opposite directions and projected onto two position- and time-sensitive microchannel plate (MCP) detectors with hexagonal delay-line position readout. The detection solid angle for the doubly and singly charged parent ions is 4π, and the acceptance angle for detection of electrons up to an energy of 20 eV is also close to 4π. However, the fragment O^+ and N^+ ions are not fully detected here due to the high momenta of these ions from the dissociation processes. Two-dimensional positions and TOFs of charged particles can be recorded by time-to-digital converters. Finally, the initial momentum vectors and consequently kinetic energies of the electrons and ions are reconstructed from the measured TOFs and positions of particle hits on the detectors.

The ions with different m/q ratios are first identified from the TOF spectrum (called TOF condition) where the ion TOFs are dependent on their initial momenta and m/q ratios. Indeed, the TOF distributions are related to the longitudinal momenta of the ions, while the transverse momenta can be determined from the two-dimensional (2D) position (POS) distributions on the detector. This momentum component is directly related to the radial displacement in position spectrum with respect to the position where ions with zero transverse momentum hit on the detector [35,36,40]. In electron-impact ionization reactions, the recoil ion momenta obtained from the collision process is normally much smaller than the fragment ion momenta due to the dissociation process. Since the momenta of fragment ions can be orders of magnitude higher than the momenta of intact molecular ions, they can be discriminated with momentum boundary conditions on both TOF and POS spectra (called TOF + POS condition). Here, an efficient approach is developed to exclude the contribution of fragment O^+ (N^+) ions from the intact O_2^{2+} (N_2^{2+}) dication yields, which will be discussed in the following sections.

III. RESULTS AND DISCUSSION

As shown in Fig. 2(a), the ionic products can be identified from the measured TOF spectrum. For O_2 molecules, the singly charged O_2^+ parent ions and its isotope products $^{16}O^{17}O^+$ and $^{16}O^{18}O^+$ are well separated in the TOF spectrum, which are located at TOFs of about 42.2, 42.8, and 43.5 μs, respectively. In addition, we observe a shoulder at the longer TOF region relative to the main peak of each ion, which is attributed to the back-scattering process of the projectile [41] where the initial momentum of the ion is directed away from the detector and thus leads to a longer TOF. In particular, the relative intensity of the shoulder for the O_2^{2+} peak (centered at 29.8 μs) is remarkable in comparison with that of the O_2^+ peak. This is because the Coulomb potential of the doubly charged O_2^{2+} ion is stronger than that of the singly charged O_2^+ ion and consequently there is a higher probability for the back-scattering process.

The broad distribution of the TOF spectrum around O_2^{2+} peak (29.8 ± 1.4 μs) contains the contributions of both intact O_2^{2+} and fragment O^+ ions with identical m/q ratios. These two cations can be produced from the following reaction channels:

$$e^- + O_2 \rightarrow 3e^- + O_2^{2+} \quad (1)$$

$$\rightarrow 3e^- + O^+ + O^+, \quad (2)$$

$$e^- + O_2 \rightarrow 2e^- + O_2^{+*} \rightarrow 3e^- + O_2^{2+} \quad (3)$$

$$\rightarrow 3e^- + O^+ + O^+, \quad (4)$$

$$e^- + O_2 \rightarrow 2e^- + O_2^+ \rightarrow 2e^- + O^+ + O, \quad (5)$$

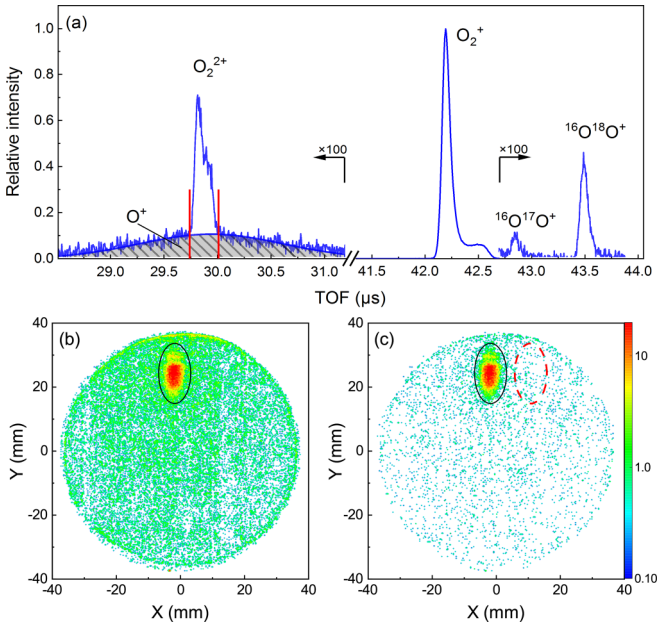

FIG. 2. (a) TOF spectra for electron-impact ($E_0 = 120$ eV) ionization of O_2 molecules. The O_2^+ peak is normalized to unity, while the intensities for other peaks are multiplied by a factor of 100 for clarity; (b) position spectrum with a broad TOF condition, i.e., 29.8 ± 1.4 μs; (c) position spectrum with a narrow TOF condition, i.e., 29.8 ± 0.2 μs.

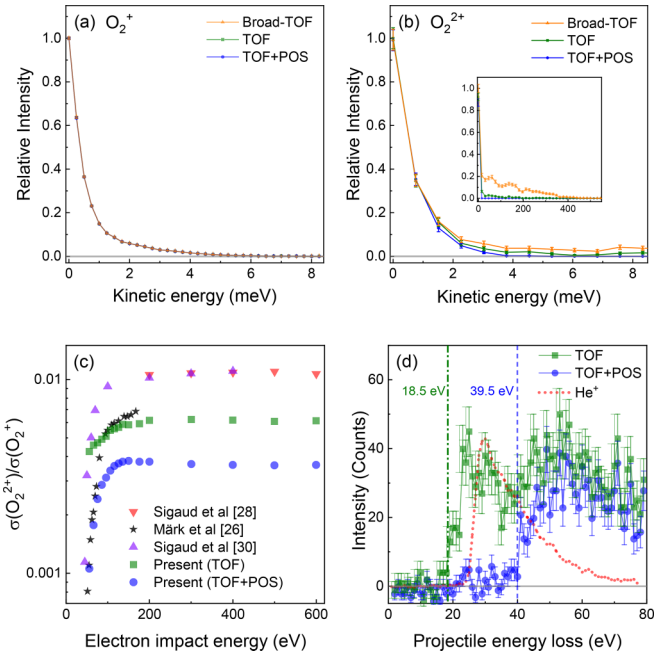

FIG. 3. (a) Measured kinetic energy spectrum for O_2^+ and (b) O_2^{2+} ions; (c) cross-section ratios between doubly and singly charged parent ions as a function of the impact energy for O_2 molecules. Previous measurements are also presented here for comparison [26,28,30]. (d) Projectile energy-loss spectra correlated to the detected ions at the incident energy of 120 eV.

where reaction channels (1)−(5) represent direct DI, direct DI plus dissociation, indirect DI (Auger process), indirect DI plus dissociation, and single-ionization plus dissociation processes, respectively. As shown in Fig. 2(a), the narrow TOF peak located at 29.8 ± 0.2 μs (red vertical lines) is mainly caused by the reaction channels (1) and (3), which lead to the intact O_2^{2+} dications. While the broad TOF distribution, i.e., the gray shaded area (29.8 ± 1.4 μs), can be attributed to the fragment O^+ ions resulting from the dissociative reaction channels (2), (4), and (5).

The 2D position distributions of the ions on the detector are presented in Figs. 2(b) and 2(c), which are obtained with the broad (29.8 ± 1.4 μs) and narrow (29.8 ± 0.2 μs) TOF conditions [see Fig. 2(a)], respectively. These 2D spectra show a small and intense elliptic structure (solid ellipse) located at the same position in both figures. This structure becomes more visible in Fig. 2(c) since the background of this figure is further suppressed with a narrow TOF condition. It is well known from Refs. [35,36,40] that the elliptic structure is mainly due to the intact O_2^{2+} dications with small recoil momenta, while the homogeneous backgrounds are attributed to the O^+ ions from the fragmentation channels. It must be stressed that the fragment O^+ ions contribute substantially to the intact O_2^{2+} yields, which cannot be eliminated with only the TOF condition, i.e., the narrow TOF peak in Fig. 2(a). Here, we propose an additional momentum boundary condition on the position spectrum of Fig. 2(c) (TOF + POS condition). First, the events in the solid ellipse are selected as the intact O_2^{2+} yields, i.e., the fragment O^+ ions beyond the solid ellipse are excluded. In addition, we further consider the contributions of O^+ in the O_2^{2+} yields by selecting the events in a equal-area ellipse of the random background region (red dashed ellipse), which are subtracted in the second step. In this way, the contributions of fragment O^+ ions are considered to be suppressed completely from the intact O_2^{2+} yields.

The momentum vectors and consequently, kinetic energies of the O_2^+ and O_2^{2+} ions are determined from the measured TOF and position spectra, which are calibrated with the ionization spectra of He^+ [shown in Fig. 3(d)]. The kinetic energy distributions of the O_2^+ and O_2^{2+} ions are shown in Figs. 3(a) and 3(b), respectively, for the broad-TOF, TOF, and TOF + POS conditions, which exhibit a sharp distribution due to the small recoil momenta of the ions and also the finite temperature of the target. In addition, the spectra show a tail structure in the higher energy region (5–400 meV), in particular for the broad-TOF condition [see inset in Fig. 3(b)], which is a signature of the O^+ ions from the dissociation processes.

For a quantitative comparison of the cross sections, both TOF and combined TOF + POS conditions are applied to obtain the yields of intact O_2^{2+} dications where the detection efficiency is also taken into account, which mainly depends on the incident energy and charge state for the individual ionic species [42,43]. The kinetic energies of the ions are increased at the time of impact on the MCP to improve the detection efficiency, which are ≈2200 eV for O_2^+ and ≈4400 eV for O_2^{2+}. Accordingly, the detection efficiencies are determined as 42.6% and 52.8% for O_2^+ and for O_2^{2+} ions, respectively [42,43]. The cross-section ratios between doubly and singly charged molecular ions, i.e., $\sigma(O_2^{2+})/\sigma(O_2^+)$, are presented in Fig. 3(c) as a function of the impact energy; also included

in the figure are the data from other experiments [26,28,30]. Here, we observe distinct differences between different experiments, particularly for the cross-section ratios above 100-eV impact energy. The data reported by Sigaud *et al.* [28,30] are higher by a factor of roughly 3 than our measurements with the TOF + POS method, while the cross-section ratios obtained by Märk [26] are in good agreement with the values derived with the TOF condition of the present work, which are higher than the present TOF + POS data by a factor of about 1.5. This indicates that the background subtraction with TOF + POS condition is roughly 50%. The deviations of $\sigma(O_2^{2+})/\sigma(O_2^+)$ ratios between different experiments are mainly caused by the fragment O^+ ions, which can contribute to the O_2^{2+} yields. The delayed extraction TOF method of Sigaud *et al.* allows the O^+ ions with higher transversal momenta to leave the extraction zone, while the O^+ ions with lower transversal momenta would be retained and eventually mixed with O_2^{2+} ions [28,30]. In addition, the deviations could also be attributed to the different TOFs of the detected ions, which are comparable to the lifetimes of the excited states of O_2^{2+} (ns to μs scale) [27,44]. In the present work, the relatively longer TOF of O_2^{2+} (29.8 μs) may cause a lower $\sigma(O_2^{2+})$ in comparison with the previous delayed extraction (TOF ≈20 μs) [28] and velocity map imaging experiments (≈2 μs) [27]. The TOF + POS approach developed in this study is considered to be an efficient way to exclude the contribution of the O^+ ions, which will be further verified in the following sections with the measured projectile energy-loss spectra in coincidence with different ionic products.

Apart from the differences in the magnitude, these experimental data show an almost identical tendency where the $\sigma(O_2^{2+})/\sigma(O_2^+)$ ratios rise rapidly with the increasing of the incident energy and reach to a constant value at higher energies ($\geqslant$120 eV). According to the first-order perturbation theory, the single-ionization cross-section of O_2^+ depends on the impact energy as $\sim(\ln E)/E$, while for the direct DI of O_2^{2+} in a two-step 2 (TS2) process where the projectile undergoes two independent collisions with two target electrons, the cross section follows a $1/E^2$ behavior [28,45,46]. Consequently, the $\sigma(O_2^{2+})/\sigma(O_2^+)$ ratios are supposed to follow a tendency of $\sim 1/(\ln E)E$ considering that O_2^{2+} is produced through a direct TS2 process. Furthermore, the $\ln E$ can be considered to vary slowly in comparison with E at high incident energies and thus, the tendency for $\sigma(O_2^{2+})/\sigma(O_2^+)$ is approximately equal to $\sim 1/E$. Regarding the indirect DI process, i.e., the inner-valence ionization and subsequent autoionization, the dependency of $\sigma(O_2^{2+})/\sigma(O_2^+)$ is approaching to a constant value with the increasing of the incident energy [28,30]. As shown in Fig. 3(c), we obtain a constant ratio for $\sigma(O_2^{2+})/\sigma(O_2^+)$ at higher energies. This indicates that the intact O_2^{2+} ions are mainly formed via the indirect DI (Auger) process, which is further confirmed by the measured projectile energy-loss spectrum.

To gain more insight into the ionization mechanisms for formation of O_2^{2+} dications, we measured the corresponding projectile energy-loss $E_{\rm loss}$ spectra, which are presented in Fig. 3(d). Here, the $E_{\rm loss}$ is defined as the incident energy minus the energy of scattered electron, i.e., $E_0 - E_1$. $E_{\rm loss} \approx$ 24.6 eV is obtained for the formation of He^+ and shown in Fig. 3(d) as the calibration for doubly and singly charged parent ions. The $E_{\rm loss}$ spectra correlated to O_2^{2+} dications are obtained with both TOF and TOF + POS conditions. The onset of $E_{\rm loss}$ with TOF condition is determined as about 18.5 eV. This value is consistent with the appearance energy of O^+ ions originating from the dissociation processes of $O_2^{+*}(b^4\Sigma_g^-)$ ion via $f^4\Pi_g$ and $d^4\Sigma_u^+$ ionic states to the first dissociation limit $O^+(^4S) + O(^3P)$ [37,47–49]. Note that the higher lying ionization and dissociation states of $b^2\Sigma_g^-$, $3^2\Pi_u$, and $c^4\Sigma_u^-$ can also contribute to the fragment O^+ ions through reaction channel (5) [47,48]. For the $E_{\rm loss}$ spectrum with the TOF + POS condition, its onset can be determined as roughly 39.5 eV, which is lying above the DI threshold of O_2 (36.13 eV) [50] and can be attributed to the $2\sigma_g$ inner-valence ionization of O_2 molecule [51,52]. Here, after the initial ionization, an outer-valence electron fills the $2\sigma_g$ inner-valence vacancy and the excess energy is released by ionizing an outer-valence electron, leading to the formation of the electronic ground state of the dications ($X^1\Sigma_g^+$) [44]. The direct DI is a minor channel here due to the geometrical constraints of the outermost π_g orbital orientation of the O_2 molecule that has low probability for the projectile to directly interact with two electrons [28,53].

Compared with the TOF + POS result, the $E_{\rm loss}$ spectrum with TOF condition shows a significant enhancement for the intensity between 18.5 and 39.5 eV, which is mainly caused by the O^+ contributions produced through reaction channel (5). The direct DI plus dissociation channel (2) and indirect DI plus dissociation channel (4) can also contribute to the O^+ ions. The O^+ ions with kinetic energy of several eV through the Coulomb explosion process [54] are barely collected in the present experiment due to the low extraction field. For indirect DI plus dissociation channel (4), the intermediate O_2^{+*} states are involved which do not autoionize to O_2^{2+} dications, but dissociate to superexcited atomic O^*. Subsequently, the O^+ ions are formed following atomic autoionization [55]. It can be seen from Fig. 3(d) that the contribution of O^+ ions is well suppressed in the $E_{\rm loss}$ spectrum with the TOF + POS condition, which provides an efficient way to obtain the yields of the intact O_2^{2+} dications.

The TOF and 2D position spectra for ionization of N_2 molecules are shown in Figs. 4(a) and 4(b), respectively. Compared with the TOF spectrum of O_2 [Fig. 2(a)], the N_2 result shows a very weak background for the intact N_2^{2+} cations. This indicates that the fragment N^+ ion is a minor contribution to the TOF spectrum of N_2^{2+}, which is also supported by the better signal-to-noise ratio of the 2D position spectrum shown in Fig. 4(b). The $\sigma(N_2^{2+})/\sigma(N_2^+)$ cross-section ratios derived with TOF and TOF + POS conditions are presented in Fig. 4(c). Both spectra show nearly identical distributions, and they are also in good agreement with the results measured with other methods [28,29]. These results further demonstrate that the experimental deviations observed for O_2 molecules [Fig. 3(c)] are mainly caused by the incomplete suppression of the O^+ species in the O_2^{2+} yields. Furthermore, the tendencies of the cross-section ratios are different between N_2 and O_2 results. In the region with energies above 100 eV, the $\sigma(N_2^{2+})/\sigma(N_2^+)$ ratios decrease linearly in a log plot with the increasing of the incident energy, which is consistent with

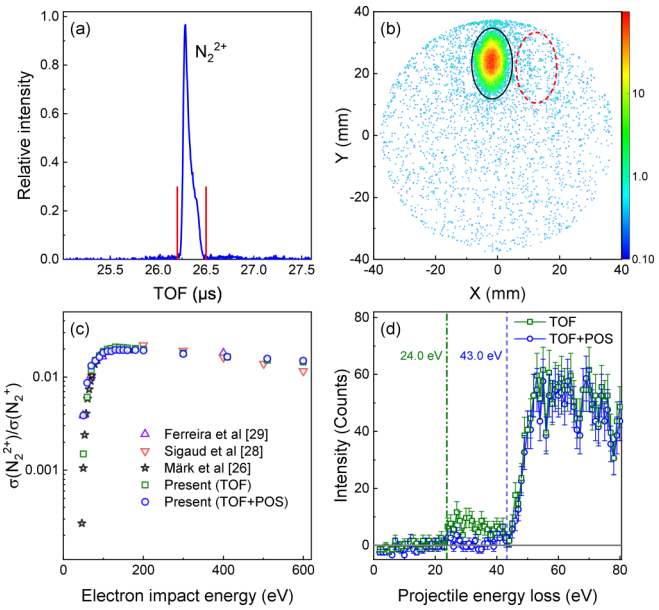

FIG. 4. (a) TOF spectrum for N_2^{2+} ions in electron-impact ionization of N_2 molecules. The peak of N_2^{2+} is normalized to unity at the maximum; (b) position spectrum with a narrow TOF condition (red vertical lines), i.e., 26.35 ± 0.15 μs; (c) cross-section ratios between doubly and singly charged parent ions for N_2 as a function of the impact energy. Previous measurements are also presented here for comparisons [26,28,29]. (d) Projectile energy-loss spectra correlated to N_2^{2+} at the incident energy of 120 eV.

the $1/E$ tendency. This indicates that the TS2 mechanism contributes significantly to the production of N_2^{2+} ions, i.e., the projectile removes two electrons in two subsequent collisions.

The energy-loss spectra provide direct evidence of the ionization mechanisms for the N_2^{2+} dications. As shown in Fig. 4(d), we determine the onsets of E_{loss} as roughly 24.0 and 43.0 eV for the spectra with TOF and TOF + POS conditions, respectively. These E_{loss} values are in line with the appearance energies of N^+ [23,34] and N_2^{2+} ions [56], respectively. It can be seen from Fig. 4(d) that there is a small hump between 24.0 and 43.0 eV energy range of the E_{loss} spectrum with TOF condition, which can be attributed to the contribution of the fragment N^+ ions produced through the dissociation of $C^2\Sigma_u^+$, $2^2\Pi_g^+$, and $D^2\Pi_g$ ionic states to the first dissociation limit of N_2^+ $(N^+(^3P) + N(^4S))$ [38,57–59]. This small contribution of N^+ to the intact N_2^{2+} dications ($\approx 5\%$) can be further suppressed with the TOF + POS condition where the onset of E_{loss} is found to be about 43.0 eV. This E_{loss} value is consistent with the DI process for the removal of two outermost electrons of N_2, which forms a $X^1\Sigma_g^+$ dicationic ground state of N_2^{2+} [56,58]. These results reveal that the direct DI mechanism are responsible for the production of the intact N_2^{2+} ions. Note that the $2\sigma_g$ inner-valence orbital ionization of N_2 (≈ 38.22 eV) does energetically not allow to initiate an autoionization process [58].

IV. CONCLUSIONS

In summary, we have studied electron-impact ionization processes of N_2 and O_2 molecules using a COLTRIMS reaction microscope. The cross-section ratios between doubly and singly charged parent ions are measured as a function of the incident energy ranging from 50 to 600 eV. We developed a method to determine accurately the cross sections for the doubly charged parent ions. Here, TOF conditions are used to determine specific ion species with identical m/q ratios, i.e., O_2^{2+} (O^+) or N_2^{2+} (N^+). Then an additional POS momentum boundary condition is utilized to exclude the possible contributions of the singly charged O^+ or N^+ fragment ions. This work provides an efficient approach to determine the absolute double-to-single ionization cross-sections of molecules and points to the reasons for the remaining noticeable discrepancies in previous measurements of the O_2^{2+} cross sections.

Moreover, the projectile energy-loss spectra are measured with an electron-ion double-coincidence method, which provides direct evidence of the ionization mechanisms of O_2 and N_2 molecules. The minimum energies leading to specific ionization channels are determined from the energy-loss distributions, where we found that N_2^{2+} dications are formed by the direct removal of two electrons from the outermost $3\sigma_g$ orbital, while O_2^{2+} dications are produced mainly by Auger decay following the $2\sigma_g$ inner-valence ionization. Furthermore, the methodology developed here can be generally applied to the studies of other molecules for which doubly charged parent ions and singly charged dissociation products have equal m/q ratios like C_2H_4, C_6H_6 and so on.

ACKNOWLEDGMENTS

This work was supported by the National Natural Science Foundation of China under Grants No. 11974272, No. 92261201, and No. 11774281. X.R. is grateful for support from the Open Fund of the State Key Laboratory of High Field Laser Physics (Shanghai Institute of Optics and Fine Mechanics).

[1] H. Ehrhardt, K. Jung, G. Knoth, and P. Schlemmer, Differential cross sections of direct single electron impact ionization, Z. Phys. D: At. Mol. Clusters **1**, 3 (1986).

[2] A. Lahmam-Bennani, Recent developments and new trends in $(e, 2e)$ and $(e, 3e)$ studies, J. Phys. B: At., Mol. Opt. Phys. **24**, 2401 (1991).

[3] E. Alizadeh, T. M. Orlando, and L. Sanche, Biomolecular damage induced by ionizing radiation: The direct and indirect effects of low-energy electrons on DNA, Annu. Rev. Phys. Chem. **66**, 379 (2015).

[4] A. G. Sanz, M. C. Fuss, A. Muñoz, F. Blanco, P. Limão-Vieira, M. J. Brunger, S. J. Buckman, and G. García, Modelling low energy electron and positron tracks for biomedical applications, Int. J. Radiat. Biol. **88**, 71 (2012).

[5] M. J. Brunger, Electron scattering and transport in biofuels, biomolecules, and biomass fragments, Int. Rev. Phys. Chem. **36**, 333 (2017).

[6] J. Zhou, X. Yu, S. Luo, X. Xue, S. Jia, X. Zhang, Y. Zhao, X. Hao, L. He, C. Wang, D. Ding, and X. Ren, Triple ionization and fragmentation of benzene trimers following ultrafast intermolecular Coulombic decay, Nat. Commun. **13**, 5335 (2022).

[7] L. Campbell and M. J. Brunger, Modelling of plasma processes in cometary and planetary atmospheres, Plasma Sources Sci. Technol. **22**, 013002 (2012).

[8] K. Bartschat and M. J. Kushner, Electron collisions with atoms, ions, molecules, and surfaces: Fundamental science empowering advances in technology, Proc. Natl. Acad. Sci. USA **113**, 7026 (2016).

[9] D. K. Böhme, Multiply-charged ions and interstellar chemistry, Phys. Chem. Chem. Phys. **13**, 18253 (2011).

[10] R. Thissen, O. Witasse, O. Dutuit, C. S. Wedlund, G. Gronoff, and J. Lilensten, Doubly-charged ions in the planetary ionospheres: A review, Phys. Chem. Chem. Phys. **13**, 18264 (2011).

[11] A. Tielens, Interstellar polycyclic aromatic hydrocarbon molecules, Annu. Rev. Astron. Astrophys. **46**, 289 (2008).

[12] L. Campbell and M. J. Brunger, Electron collisions in atmospheres, Int. Rev. Phys. Chem. **35**, 297 (2016).

[13] A. G. G. M. Tielens, The molecular universe, Rev. Mod. Phys. **85**, 1021 (2013).

[14] M. Larsson, W. D. Geppert, and G. Nyman, Ion chemistry in space, Rep. Prog. Phys. **75**, 066901 (2012).

[15] R. D. DuBois and S. T. Manson, Multiple-ionization channels in proton-atom collisions, Phys. Rev. A **35**, 2007 (1987).

[16] T. Spranger and T. Kirchner, Auger-like processes in multiple ionization of noble gas atoms by protons, J. Phys. B: At., Mol. Opt. Phys. **37**, 4159 (2004).

[17] B. Gaire, D. J. Haxton, F. P. Sturm, J. Williams, A. Gatton, I. Bocharova, N. Gehrken, M. Schöffler, H. Gassert, S. Zeller, J. Voigtsberger, T. Jahnke, M. Zohrabi, D. Reedy, C. Nook, A. L. Landers, A. Belkacem, C. L. Cocke, I. Ben-Itzhak, R. Dörner, and T. Weber, Auger decay and subsequent fragmentation pathways of ethylene following K-shell ionization, Phys. Rev. A **92**, 013408 (2015).

[18] P. Liu, Y. Liu, and J. Zeng, Auger decay and the direct double ionization probability of a $2p$ inner-shell hole in a singly charged Ar^+ ion, Eur. Phys. J. D **68**, 214 (2014).

[19] E. G. Cavalcanti, G. M. Sigaud, E. C. Montenegro, M. M. Sant'Anna, and H. Schmidt-Böcking, Post-collisional effects in multiple ionization of neon by protons, J. Phys. B: At., Mol. Opt. Phys. **35**, 3937 (2002).

[20] S. W. J. Scully, J. A. Wyer, V. Senthil, M. B. Shah, and E. C. Montenegro, Autodissociation of doubly charged water molecules, Phys. Rev. A **73**, 040701(R) (2006).

[21] N. D. Cariatore, N. Bachi, and S. Otranto, C^{6+}-impact ionization of uracil at MeV/u impact energies: The role of the multiple-ionization channel, Phys. Rev. A **106**, 012808 (2022).

[22] Y. Itikawa, Cross sections for electron collisions with oxygen molecules, J. Phys. Chem. Ref. Data **38**, 1 (2009).

[23] Y. Itikawa, Cross sections for electron collisions with nitrogen molecules, J. Phys. Chem. Ref. Data **35**, 31 (2006).

[24] A. I. Lozano, A. García-Abenza, F. Blanco Ramos, M. Hasan, D. S. Slaughter, T. Weber, R. P. McEachran, R. D. White, M. J. Brunger, P. Limão-Vieira, and G. García Gómez-Tejedor, Electron and positron scattering cross sections from CO_2: A comparative study over a broad energy range (0.1–5000 eV), J. Phys. Chem. A **126**, 6032 (2022).

[25] S. Halas and B. Adamczyk, Cross sections for the production of N_2^+, N^+, and N_2^{2+} from nitrogen by electrons in the energy range 16–600 eV, Int. J. Mass Spectrom. Ion Phys. **10**, 157 (1972).

[26] T. D. Märk, Cross section for single and double ionization of N_2 and O_2 molecules by electron impact from threshold up to 170 eV, J. Chem. Phys. **63**, 3731 (1975).

[27] J. N. Bull, J. W. L. Lee, and C. Vallance, Electron ionization dynamics of N_2 and O_2 molecules: Velocity-map imaging, Phys. Rev. A **91**, 022704 (2015).

[28] L. Sigaud and E. C. Montenegro, Highly selective mechanisms for the production of N_2 and O_2 dications by electron impact, Phys. Rev. A **98**, 052701 (2018).

[29] N. Ferreira, L. Sigaud, V. L. B. de Jesus, A. B. Rocha, L. H. Coutinho, and E. C. Montenegro, Fragmentation of $^{14,15}N_2$ by electron impact investigated using a time-delayed spectroscopic technique, Phys. Rev. A **86**, 012702 (2012).

[30] L. Sigaud, N. Ferreira, and E. C. Montenegro, Absolute cross sections for O_2 dication production by electron impact, J. Chem. Phys. **139**, 024302 (2013).

[31] W. Wolff, A. Perlin, R. R. Oliveira, F. Fantuzzi, L. H. Coutinho, F. de A Ribeiro, and G. Hilgers, Production of long-lived benzene dications from electron impact in the 20–2000 eV energy range combined with the search for global minimum structures, J. Phys. Chem. A **124**, 9261 (2020).

[32] L. Sigaud, W. Wolff, and E. C. Montenegro, Strong isotopic selectivity on dication formation of benzene, Phys. Rev. A **105**, 032816 (2022).

[33] C. Tian and C. R. Vidal, Electron impact ionization of N_2 and O_2: Contributions from different dissociation channels of multiply ionized molecules, J. Phys. B: At., Mol. Opt. Phys. **31**, 5369 (1998).

[34] C. Wu, Y. Yang, Z. Wu, B. Chen, H. Dong, X. Liu, Y. Deng, H. Liu, Y. Liu, and Q. Gong, Coulomb explosion of nitrogen and oxygen molecules through non-Coulombic states, Phys. Chem. Chem. Phys. **13**, 18398 (2011).

[35] R. Dörner, V. Mergel, O. Jagutzki, L. Spielberger, J. Ullrich, R. Moshammer, and H. Schmidt-Böcking, Cold target recoil ion momentum spectroscopy: A "momentum microscope" to view atomic collision dynamics, Phys. Rep. **330**, 95 (2000).

[36] J. Ullrich, R. Moshammer, A. Dorn, R. Dörner, L. P. H. Schmidt, and H. Schmidt-Böcking, Recoil-ion and electron momentum spectroscopy: Reaction microscopes, Rep. Prog. Phys. **66**, 1463 (2003).

[37] N. Watanabe, S. Yamada, and M. Takahashi, $(e, e + \text{ion})$ study on electron-induced dissociative ionization of O_2, Phys. Rev. A **99**, 022704 (2019).

[38] N. Watanabe, S. Yamada, and M. Takahashi, Stereodynamics of electron-induced dissociative ionization of N_2 studied by $(e, e + \text{ion})$ spectroscopy, Phys. Chem. Chem. Phys. **20**, 1063 (2018).

[39] X. Ren, J. Zhou, E. Wang, T. Yang, Z. Xu, N. Sisourat, T. Pfeifer, and A. Dorn, Ultrafast energy transfer between π-stacked aromatic rings upon inner-valence ionization, Nat. Chem. **14**, 232 (2022).

[40] A. Dorn, M. Weyland, and X. Ren, Electron-ion momentum vector coincidences in electron collisions with atoms and molecules, J. Electron Spectrosc. Relat. Phenom. **230**, 33 (2019).

[41] S. Yan, X. Ma, P. Zhang, S. Xu, S. F. Zhang, X. L. Zhu, W. T. Feng, and H. P. Liu, Signatures of the projectile electron–target

core elastic scattering in Ar (e, $2e$) reactions at low and intermediate impact energies, J. Phys. B: At., Mol. Opt. Phys. **44**, 055202 (2011).

[42] L. Sigaud, V. L. B. de Jesus, N. Ferreira, and E. C. Montenegro, A novel double-focusing time-of-flight mass spectrometer for absolute recoil ion cross sections measurements, Rev. Sci. Instrum. **87**, 083112 (2016).

[43] N. Takahashi, Y. Adachi, M. Saito, and Y. Haruyama, Absolute detection efficiencies for keV energy atoms incident on a microchannel plate detector, Nucl. Instrum. Methods Phys. Res., Sect. B **315**, 51 (2013).

[44] M. Lundqvist, D. Edvardsson, P. Baltzer, M. Larsson, and B. Wannberg, Observation of predissociation and tunnelling processes in O_2^{2+}: A study using Doppler free kinetic energy release spectroscopy and *ab initio* CI calculations, J. Phys. B: At., Mol. Opt. Phys. **29**, 499 (1996).

[45] L. Sigaud and E. C. Montenegro, Branching ratios for the fragmentation pathways leading to $C_2H_4^+$ in electron–ethylene collisions, J. Phys. B: At., Mol. Opt. Phys. **50**, 105202 (2017).

[46] H. Luna, W. Wolff, E. C. Montenegro, and L. Sigaud, CH_4 fragmentation from single and double ionization by proton and electron impact, Phys. Rev. A **99**, 012709 (2019).

[47] Y. Hikosaka, T. Aoto, R. I. Hall, and K. Ito, Fragment emission anisotropy in the dissociative photoionization of O_2 investigated by two-dimensional photoion spectroscopy, J. Phys. B: At., Mol. Opt. Phys. **36**, 1423 (2003).

[48] Y. Lu, Z. He, J. Cutler, S. Southworth, W. Stolte, and J. Samson, Dissociative photoionization study of O_2, J. Electron Spectrosc. Relat. Phenom. **94**, 135 (1998).

[49] X. Tang, G. A. Garcia, and L. Nahon, New insights onto dissociation of state-selected O_2^+ ions investigated by double imaging photoelectron photoion coincidence: The superimposed $3^2\Pi_u^-$ and $c^4\Sigma_u^-$ inner-valence states, J. Chem. Phys. **148**, 124309 (2018).

[50] R. I. Hall, G. Dawber, A. McConkey, M. A. MacDonald, and G. C. King, Vibrational Structure of the O_2^{2+} Ground State Observed by Threshold Photoelectron Coincidence Spectroscopy, Phys. Rev. Lett. **68**, 2751 (1992).

[51] P. Lin and R. R. Lucchese, Theoretical studies of cross sections and photoelectron angular distributions in the valence photoionization of molecular oxygen, J. Chem. Phys. **116**, 8863 (2002).

[52] Y. Hikosaka, T. Aoto, R. I. Hall, K. Ito, R. Hirayama, N. Yamamoto, and E. Miyoshi, Inner-valence states of O_2^+ and dissociation dynamics studied by threshold photoelectron spectroscopy and a configuration interaction calculation, J. Chem. Phys. **119**, 7693 (2003).

[53] A. S. Alnaser, S. Voss, X. M. Tong, C. M. Maharjan, P. Ranitovic, B. Ulrich, T. Osipov, B. Shan, Z. Chang, and C. L. Cocke, Effects of Molecular Structure on Ion Disintegration Patterns in Ionization of O_2 and N_2 by Short Laser Pulses, Phys. Rev. Lett. **93**, 113003 (2004).

[54] A. S. Sandhu, E. Gagnon, R. Santra, V. Sharma, W. Li, P. Ho, P. Ranitovic, C. L. Cocke, M. M. Murnane, and H. C. Kapteyn, Observing the creation of electronic Feshbach resonances in soft x-ray-induced O_2 dissociation, Science **322**, 1081 (2008).

[55] R. Feifel, J. H. D. Eland, and D. Edvardsson, Valence double ionization of O_2 at photon energies below and above the molecular double ionization threshold, J. Chem. Phys. **122**, 144308 (2005).

[56] H. R. Koslowski, H. Lebius, V. Staemmler, R. Fink, K. Wiesemann, and B. A. Huber, Collisions of doubly charged nitrogen molecules with rare gas atoms, J. Phys. B: At., Mol. Opt. Phys. **24**, 5023 (1991).

[57] T. Aoto, K. Ito, Y. Hikosaka, A. Shibasaki, R. Hirayama, N. Yamamono, and E. Miyoshi, Inner-valence states of N_2^+ and the dissociation dynamics studied by threshold photoelectron spectroscopy and configuration interaction calculation, J. Chem. Phys. **124**, 234306 (2006).

[58] D. Bhattacharya, K. R. Shamasundar, and A. Emmanouilidou, Potential energy curves of molecular nitrogen for singly and doubly ionized states with core and valence holes, J. Phys. Chem. A **125**, 7778 (2021).

[59] S. Armenta Butt and S. D. Price, Bond-forming and electron-transfer reactivity between Ar^{2+} and N_2, Phys. Chem. Chem. Phys. **23**, 11287 (2021).